Cell

Comparative Epigenomic Analysis of Murine and Human Adipogenesis

Tarjei S. Mikkelsen,[1,4] Zhao Xu,[1,2,4] Xiaolan Zhang,[1] Li Wang,[1] Jeffrey M. Gimble,[3] Eric S. Lander,[1] and Evan D. Rosen[1,2,*]
[1]Broad Institute, 7 Cambridge Center, Cambridge, MA 02142, USA
[2]Division of Endocrinology and Metabolism, Beth Israel Deaconess Medical Center, 330 Brookline Avenue, Boston, MA 02115, USA
[3]Stem Cell Biology Laboratory, Pennington Biomedical Research Center, Louisiana University System, 6400 Perkins Road, Baton Rouge, LA 70808, USA
[4]These authors contributed equally to this work
*Correspondence: erosen@bidmc.harvard.edu
DOI 10.1016/j.cell.2010.09.006

SUMMARY

We report the generation and comparative analysis of genome-wide chromatin state maps, PPARγ and CTCF localization maps, and gene expression profiles from murine and human models of adipogenesis. The data provide high-resolution views of chromatin remodeling during cellular differentiation and allow identification of thousands of putative preadipocyte- and adipocyte-specific *cis*-regulatory elements based on dynamic chromatin signatures. We find that the specific locations of most such elements differ between the two models, including at orthologous loci with similar expression patterns. Based on sequence analysis and reporter assays, we show that these differences are determined, in part, by evolutionary turnover of transcription factor motifs in the genome sequences and that this turnover may be facilitated by the presence of multiple distal regulatory elements at adipogenesis-dependent loci. We also utilize the close relationship between open chromatin marks and transcription factor motifs to identify and validate PLZF and SRF as regulators of adipogenesis.

INTRODUCTION

Describing the gene regulatory networks (GRNs) that control development, differentiation, and physiological processes is a major goal of mammalian genome biology. A GRN consists of *trans*-regulatory factors and *cis*-regulatory elements whose interactions with each other and the environment govern the expression of genes in the network and ultimately manifest as a complex phenotype such as gastrulation, adipogenesis, or glucose homeostasis (Arnone and Davidson, 1997). The core *trans*-regulatory factors in a variety of GRNs have been identified by expression profiling and genetic analysis, but the large size and complex architecture of mammalian genomes have prevented systematic identification of *cis*-regulatory elements.

Recent advances in high-throughput DNA sequencing have led to the development of new experimental tools that greatly enhance our ability to study genome function. In particular, chromatin immunoprecipitation and sequencing (ChIP-Seq) allows efficient genome-wide profiling of transcription factor (TF) localization (Johnson et al., 2007; Robertson et al., 2007) and chromatin state (Barski et al., 2007; Mikkelsen et al., 2007a). Because different classes of *cis*-regulatory elements display characteristic chromatin signatures when they are active (Hon et al., 2009), ChIP-Seq has emerged as a powerful tool for comprehensive discovery of these elements.

Identifying the components of a GRN that govern a specific phenotype of interest from ChIP-Seq maps of a given cell type, however, remains challenging for several reasons. First, these maps typically identify tens of thousands of putative regulatory elements, only some of which are likely to be directly relevant to the phenotype. Second, whereas these maps appear to be highly sensitive, their specificity toward biologically relevant elements is less clear (Birney et al., 2007). For example, TF localization analyses frequently reveal many binding sites that have no discernable effect on the expression levels of nearby genes (Johnson et al., 2007; Robertson et al., 2007; Zhang et al., 2005). Third, practical considerations often necessitate the use of in vitro cell culture models that might be subject to aberrant genetic or epigenetic changes. This raises the possibility that some chromatin state components observed in an in vitro model may not be representative of the analogous cell type in vivo (Noer et al., 2009).

We reasoned that comparative profiling of multiple cell culture models that display similar, inducible phenotypes might help shed light on these issues. Profiling closely related cell types before and after induction should help identify regulatory elements that are directly related to the phenotype. Classification of these elements as either model-specific or shared should then provide a foundation for understanding their relative importance and therefore help prioritize in-depth functional studies.

To explore this approach, we focused on adipogenesis. Adipocytes play a central role in systemic metabolism, coordinating lipid and glucose homeostasis (Rosen and Spiegelman, 2006). The burgeoning human and financial costs of obesity, type 2 diabetes, and other metabolic disorders have therefore thrust adipocyte biology into the forefront of biomedical research

priorities (Camp et al., 2002). Adipogenesis is also one of the most intensively studied examples of cellular differentiation, and several cell culture models that appear to closely approximate events that occur during adipogenesis in vivo are available (Rosen and MacDougald, 2006).

Here, we report the generation and analysis of genome-wide chromatin state maps, TF localization maps, and gene expression profiles from multiple stages of differentiation in two established models of adipogenesis, murine 3T3-L1 cells (L1s) and human adipose stromal cells (hASCs). 3T3-L1 is a cell line originally subcloned from embryonic fibroblasts (Green and Meuth, 1974), and hASCs are primary cells derived from adult subcutaneous lipoaspirates (Aust et al., 2004). Undifferentiated L1s and hASCs ("preadipocytes") have similar fibroblast-like morphologies. When induced to undergo terminal differentiation in adipogenic media, both change into round cells that exhibit properties typical of adipocytes in vivo, such as insulin-stimulated glucose uptake, lipogenesis, catecholamine-stimulated lipolysis, and adipokine secretion. These two models therefore provide the opportunity to study GRNs that govern similar adipogenic phenotypes against a background of phylogenetic, ontogenetic and technical differences.

RESULTS

Comparative Epigenomic Profiling of Adipogenesis

To facilitate comprehensive epigenomic profiling of cells undergoing adipogenesis, we expanded L1 and hASC preadipocytes and induced differentiation in adipogenic media. We selected four matched time points that represented similar stages of differentiation, as judged by morphology and lipid droplet accumulation. These time points corresponded to proliferating (day −2) and confluent (day 0) preadipocytes, immature adipocytes (day 2 for L1s, day 3 for hASCs), and mature adipocytes (day 7 for L1s, day 9 for hASCs).

We generated genome-wide chromatin state maps using ChIP-Seq, profiling six histone modifications (H3K4me3/me2/me1, H3K27me3/ac, and H3K36me3) and the CCCTC-binding factor (CTCF) at all four time points. We also profiled the adipogenic TF peroxisome proliferators-activated receptor γ (PPARγ) at the last time point. The resulting data consist of 60 ChIP-Seq experiments and two negative controls. We also measured mRNA and miRNA expression levels in both models using microarrays. All data have been deposited in public databases.

To visualize the data, we generated histograms of normalized densities of ChIP fragments across the genomes. Figure 1 shows these densities near the murine *Pparg* gene, which is strongly upregulated during adipogenesis (Figure S1, available online, shows the human *PPARG* locus). The profiled histone modifications and TFs showed spatial and temporal density distributions that are qualitatively consistent with their known functions (Hon et al., 2009). For example, H3K4me3, which is associated with transcriptional initiation, was primarily found near known promoters. A case in point is the gain of H3K4me3 observed near the adipocyte-specific alternative promoter of *Pparg* (P2, Figure 1). H3K4me2/me1 and H3K27ac, which are associated with "open" chromatin and *cis*-regulatory activity, showed dynamic distributions in promoter, intronic, and intergenic regions. H3K36me3, which is associated with transcriptional elongation, was distributed across active gene bodies and increased markedly across *Pparg* as it was upregulated. H3K27me3, which is associated with Polycomb-mediated repression, was distributed broadly across the inactive flanking regions. The PPARγ and CTCF densities showed sharp peaks, consistent with individual TF binding sites.

To support quantitative analyses, we identified significant clusters of ChIP fragments using a sliding window approach for histone modifications and QuEST (Valouev et al., 2008) for TF-binding sites. Each such region or binding site was assigned an "enrichment score," which represents the ratio of observed over expected fragments. Their genome-wide distributions are consistent with the qualitative patterns described above (Table S1). mRNA and miRNA expression analyses revealed correlated expression dynamics that are consistent with efficient adipogenic differentiation (Figure S2, Table S2, and Extended Experimental Procedures).

To compare data from the two models, we first attempted to map each enriched region in the mouse genome to corresponding regions of orthologous sequence in the human genome, and vice versa, using previously computed whole-genome alignments. About 80%–90% of these regions could be mapped to the other genome. We then asked whether these orthologous regions overlapped the same chromatin marks or TF-binding sites in the other model (conservatively requiring an overlap of $\geq$ 1 bp). We will refer to such overlaps as "shared" marks or binding sites and the remainder as "model-specific."

We conclude that the data provide a rich resource for studies of chromatin remodeling and gene regulation in two key models of adipogenesis. In the following sections, we focus on detection and functional analysis of *cis*-regulatory elements in the adipogenic GRN and the sequence-specific TFs that interact with them.

Histone Modifications Associated with Distal Enhancers

We began our analysis by characterizing open chromatin marks in regions distal to (>2 kb from) known promoters. H3K4me2/me1 and H3K27ac were distributed in highly correlated patterns at each time point and changed dynamically in thousands of genomic regions in each cell culture model (Table S1). These "dynamic" regions were often clustered near genes with adipogenesis-dependent expression patterns, suggesting that they represent cooperative or redundant distal enhancers. Orthologous genes with similar expression in L1s and hASCs frequently showed similar chromatin marks, but the specific location of these marks was often model specific; this suggests that the expression pattern of genes is better conserved between the models than the specific elements controlling the expression.

To identify putative distal enhancers, we focused on H3K27ac because recruitment of histone acetyltransferases (HATs) is the most specific signature known for these elements (Ghisletti et al., 2010; Heintzman et al., 2009; Wang et al., 2008). We detected 29,092 distal H3K27ac regions in L1 adipocytes (day 7), with enrichment scores spanning an order of magnitude (Table S3). Of these, 6096 (~21%) showed a $\geq$ 5-fold increase in enrichment scores relative to preadipocytes (days −2 and 0), suggesting that they harbor regulatory elements that recruit HATs during adipogenesis. Conversely, we identified 5159

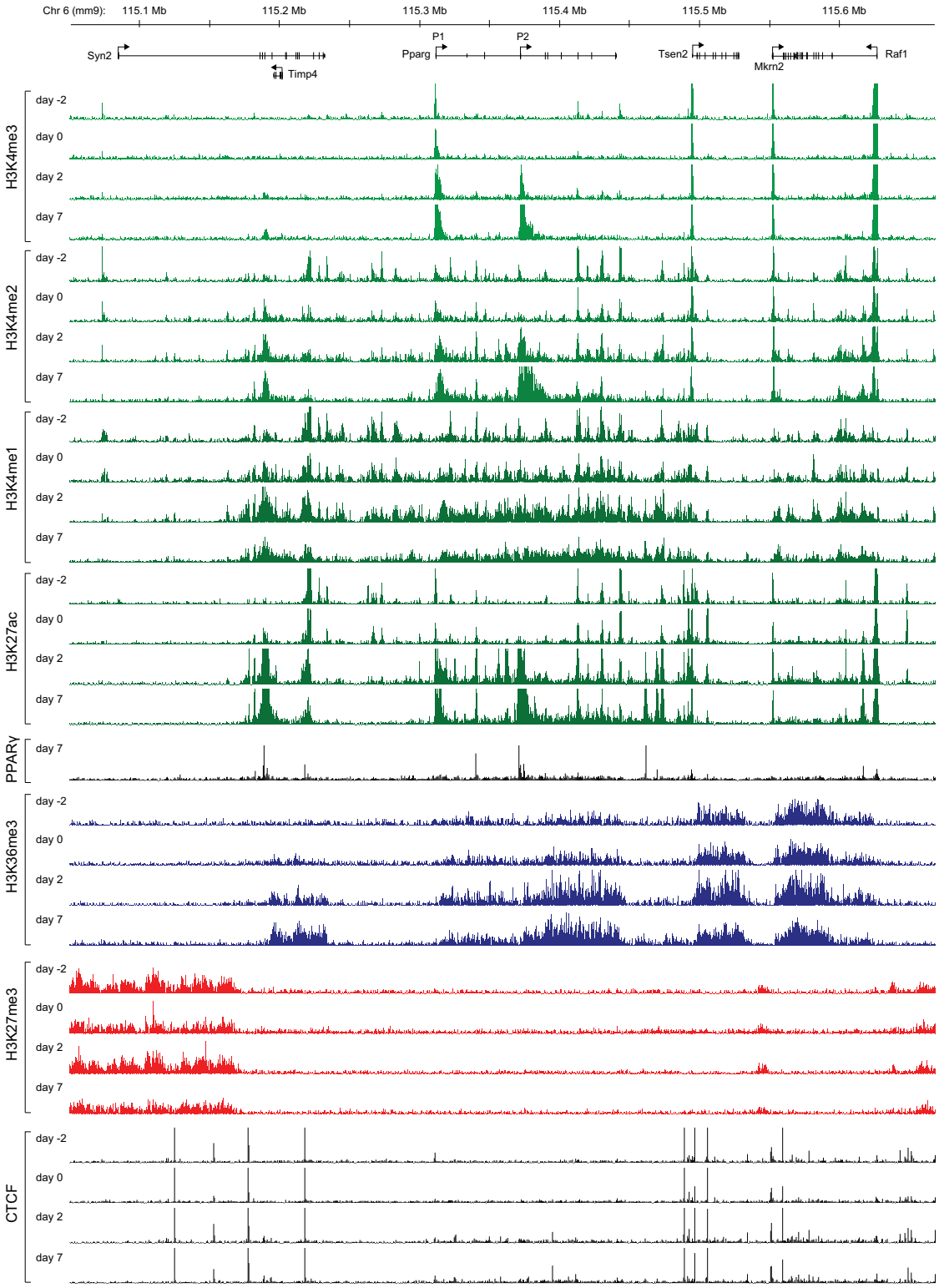

Figure 1. Chromatin State and TF Localization Near *Pparg* during L1 Adipogenesis

Histograms of ChIP fragments across the *Pparg* locus, normalized to fragments per 10 million aligned reads, for each of the profiled histone modifications and TFs at four time points during L1 adipogenesis. All histograms are shown on the same scale, and high values were truncated as necessary. See also Figure S1 and Figure S2 and Table S1 and Table S2.

H3K27ac regions in L1 preadipocytes (day −2) whose enrichment scores decreased at least 5-fold. We observed similar dynamics in hASCs (Table S3).

Dynamic changes in open chromatin marks were significantly correlated with changes in the expression levels of linked genes. For simplicity, we assumed that each H3K27ac region was associated with the closest known gene (although there are counterexamples, as described below). Roughly 15% of all genes on our microarrays showed a ≥ 2-fold change in expression between L1 adipocytes and preadipocytes. We found that the more the expression level of a gene increased or decreased, the more likely it was to be associated with adipocyte- or preadipocyte-specific H3K27ac, respectively (Figure 2A). Conversely, the likelihood that the expression level of a gene changed ≥ 2-fold was positively correlated with both the enrichment scores (Figure 2B) and the total number (Figure 2C) of dynamic H3K27ac regions associated with it. By contrast, association with invariant H3K27ac (enriched in both adipocytes and preadipocytes) had little predictive value with respect to changes in expression. We observed similar patterns in hASCs (Figures 2D–2F). Distal regions that show changes in open chromatin marks during adipogenesis are therefore likely to be enriched for cell type-specific enhancers. Moreover, genes with dynamic expression patterns appear to frequently be located near multiple such enhancers (see below and Figure S3).

Comparing open chromatin marks between L1s and hASCs, we found that ~15%–30% of marks identified in one model were shared with the other model (that is, orthologous sequences contained the same chromatin marks). Given that regions enriched for each open chromatin mark only covered ~2%–4% of each genome, this represents a highly significant degree of overlap. Regions with the same size distributions randomly placed across the two genomes would have an expected overlap of less than 0.5%. Nevertheless, the majority (70%–85%) of distal open chromatin marks were model specific.

Orthologs that were only associated with dynamic open chromatin marks in one of the models often showed discordant expression patterns. For example, orthologs whose expression increased more in L1s than in hASCs were also more likely to be associated with adipocyte-specific H3K27ac only in L1s and vice versa (Figure 2G). This suggests that model-specific open chromatin marks correlate with model-specific enhancers. Of interest, orthologous genes with similar expression patterns often had similar chromatin marks nearby, but the specific locations of these marks were typically model specific. For example, at orthologous loci induced ≥ 2-fold in both models, the majority (84%) of adipocyte-specific H3K27ac regions in L1s were not shared with hASCs and vice versa. Their expression patterns therefore appear to be better conserved than the specific enhancers that regulate them (below, we verify this observation through functional analyses).

PPARγ Localization

We next analyzed the distribution of binding sites for PPARγ in mature L1 and hASC adipocytes (day 7/9). PPARγ is a nuclear receptor that is recruited to PPAR response elements (PPREs) during adipogenesis as a heterodimer with retinoid X receptors (RXRs) (Ijpenberg et al., 1997) and primarily functions as a transcriptional activator (Lefterova et al., 2008; Nielsen et al., 2008). We found that PPARγ was largely localized to distal regions enriched for open chromatin marks. The vast majority of PPARγ-binding sites were not shared between L1s and hASCs, and this could be explained, in part, by turnover of its motif in the genome sequences. Loci with PPARγ-binding sites in both L1s and hASCs were, however, highly enriched for genes with functions relevant to known adipocyte biology.

We detected 7,142 and 39,986 PPARγ-binding sites in L1s and hASCs, respectively (1% FDR; Table S4), with enrichment scores spanning two orders of magnitude. The excess number of human sites primarily reflects the identification of more weak binding sites (Extended Experimental Procedures). Performing ChIP-Seq with a different PPARγ antibody yielded similar results, and the L1 sites reported here showed good concordance with 5299 sites previously detected in this model using ChIP-chip (Lefterova et al., 2008; Figure S4).

The PPARγ-binding sites followed qualitatively similar patterns in L1s and hASCs, with the vast majority (85%–95%) overlapping open chromatin marks (Figure 3A). Ab initio motif discovery recovered motifs that were similar to the canonical PPARγ/RXR DR1 motif (Figure 3B). There are, however, ~1.5 million instances of these motifs in each genome; this implies that we detected PPARγ binding at only ~1 in 200 motifs in the mouse genome. Other factors must therefore contribute to binding site selectivity. Of note, a motif instance was ~15 times more likely be bound by PPARγ in L1 adipocytes if it overlapped a region enriched for open chromatin marks in preadipocytes ($p_{Fisher} < 10^{-60}$). In fact, ~77% of all PPARγ-binding sites detected in L1s were located in such regions. This suggests that PPARγ recruitment during adipogenesis is strongly influenced by the preadipocyte chromatin state.

The majority (79%) of sites bound by PPARγ in L1s were not shared with hASCs, despite the larger number of sites detected in the latter model. Of note, 34% of L1 PPARγ-binding sites that could not be mapped to the human genome resided within rodent-specific transposable element insertions, which implies that they evolved after the mouse and human lineages diverged. If an L1-binding site could be mapped to an orthologous human sequence, the presence of PPARγ binding in hASCs correlated with the presence a conserved motif and open chromatin marks (Figure 3C). Evolutionary turnover of DR1-like motifs is therefore likely to contribute to the differential recruitment of PPARγ and open chromatin marks between the two models.

To explore the correlation between PPARγ recruitment and gene expression, we again assumed that each binding site was associated with the closest known protein-coding gene. We found that genes associated with PPARγ in L1s were approximately three times more likely than nonassociated genes to be upregulated ≥ 2-fold ($p_{Fisher} < 10^{-60}$). The majority (84%) of genes associated with PPARγ-binding sites were not upregulated, but the likelihood that a gene was upregulated increased when an associated PPARγ binding site had a higher ChIP enrichment score; was shared with hASCs; or overlapped adipocyte-specific H3K27ac (Figure 3D). The correlation between upregulation and gain of H3K27ac is notable. It suggests that, whereas PPARγ binding is biased toward regions

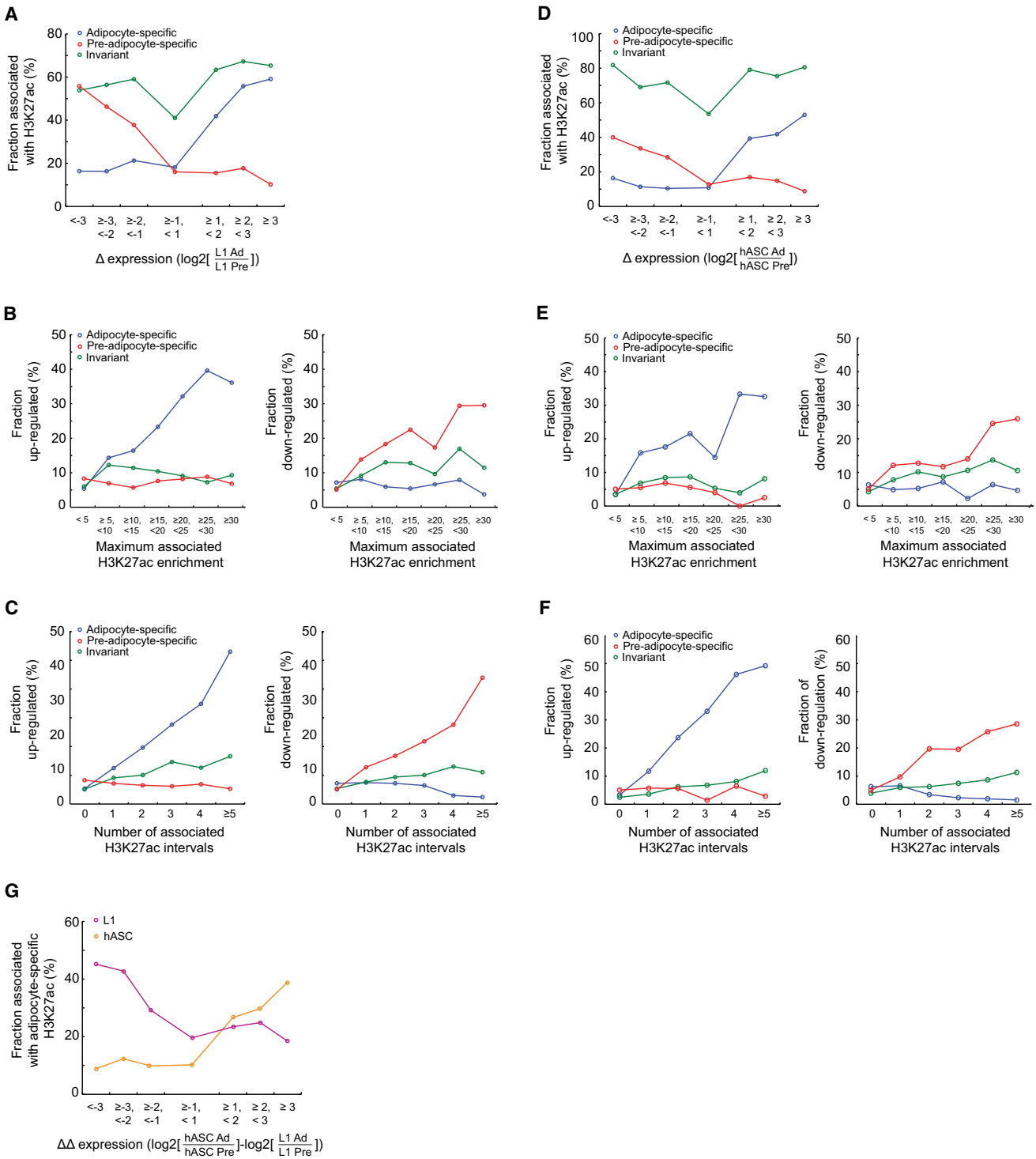

Figure 2. Histone Modifications and Distal *cis*-Regulatory Elements

(A) Fractions of genes associated with at least one adipocyte (Ad), preadipocyte (Pre), or invariant H3K27ac region in L1s, conditional on changes in expression levels in adipocytes (max of days 2 and 7) relative to preadipocytes (max of days −2 and 0).

(B) Fractions of genes that showed ≥ 2-fold upregulation (left) or downregulation (right) in L1s, conditional on the maximal enrichment score of associated H3K27ac regions.

(C) Fractions of genes that showed ≥ 2-fold upregulation (left) or downregulation (right) in L1s, conditional on the number of associated H3K27ac regions.

(D) Fractions of genes associated with at least one H3K27ac region in hASCs, conditional on their changes in expression levels in adipocytes (max [day 3/9]) relative to preadipocytes (max [day −2/0]).

that were already acetylated in preadipocytes, PPARγ-binding sites that recruit HATs to new locations are more likely to be functionally relevant.

Concentrating on genes with "dynamic" PPARγ-binding sites that gain H3K27ac in L1s, we found that those for which the orthologous human gene was *not* associated with H3K27ac in hASCs were significantly more likely to show greater upregulation in L1s than in hASCs and vice versa ($p_{Fisher} < 10^{-4}$; Figure 3E). Model-specific PPREs are therefore likely to contribute to differential gene regulation in the two models. Annotation enrichment analysis (Dennis et al., 2003) revealed, however, that genes that were associated with PPARγ-binding sites and upregulated in both models were strongly enriched for components of the classic PPARγ signaling pathway, as well as essential adipocyte functions related to lipid metabolism and cellular respiration (Figure 3F). Of note, only ~57% of these concordantly upregulated genes actually shared orthologous PPARγ-binding sites. Thus, PPARγ targeting of adipocyte genes appears to be better conserved than the specific PPREs that mediate PPARγ recruitment to these genes.

CTCF Localization

We next analyzed the distribution of binding sites for CTCF, a DNA-binding protein that plays a key role in higher-order organization of chromatin and is associated with insulator and enhancer-blocking activities (Phillips and Corces, 2009). We found that CTCF recruitment was relatively invariant during differentiation in each model but that the specific binding sites differed significantly between the two models. These differences appear to be largely caused by evolutionary turnover of CTCF motifs.

We detected ~43,000 CTCF-binding sites at each time point in each model (1% FDR). The sites followed largely intergenic distributions similar to those described in other cell types (Barski et al., 2007; Kim et al., 2007; Xi et al., 2007; Figure 3G). *Ab initio* motif discovery recovered the known CTCF motif (Figure 3H), and most (~84%) binding sites overlapped a good match to this motif. Less than half overlapped H3K27ac or H3K4 methylation, suggesting that these open chromatin marks are not directly linked to CTCF localization. Most CTCF-binding sites detected at one time point were also detected at other time points. For example, ~84% of CTCF-binding sites in mature L1 adipocytes were also bound in L1 preadipocytes.

In contrast, among the ~70% of binding sites in L1s that could be mapped to orthologous regions in the human genome, only about half (~53%) were also bound in hASCs. Shared CTCF binding in hASCs was strongly correlated with the presence of a conserved CTCF motif in the human genome (Figure 3I). As was the case for PPARγ, among the remaining ~30% of CTCF-binding sites in L1s that could not be mapped, ~65%, including thousands of the most strongly enriched sites, were located within rodent-specific transposon insertions.

Functional and Comparative Analysis of the *Cd36/CD36* Locus

In the previous sections, we largely relied on genome-wide statistical analysis. To explore the relationships between open chromatin marks, TF localization, and *cis*-regulatory elements in greater depth, we focused on the *Cd36/CD36* locus. This PPARγ-responsive gene encodes a long-chain fatty acid receptor expressed in adipocytes and other cell types (Yu et al., 2003) and was one of the most strongly induced genes in both L1s and hASCs. We confirmed the activity of multiple adipocyte-specific promoters and enhancers predicted by the L1 chromatin state maps using functional assays. Consistent with our genome-wide results, comparative analysis revealed that, whereas the *Cd36/CD36* expression pattern is similar between L1s and hASCs, several *cis*-regulatory elements active in L1s are not conserved in the human genome.

We first analyzed the murine *Cd36* locus, which contains three promoters (P1–P3, Figure 4A) and encodes five transcripts with identical coding sequences. In preadipocytes, we detected three CTCF-binding sites flanking the locus but little enrichment for any of the histone modifications. In adipocytes, we detected H3K4me3 at P2 and P3, suggesting that these are the major promoters used in L1s. To confirm this, we quantified each *Cd36* isoform using RT-qPCR. As expected, the vast majority (~99%) of transcripts originated from P2 and P3 (Figure S5A). We detected six adipocyte-specific H3K27ac regions across a ~150 kb region upstream of the two active promoters, five of which also contained PPARγ-binding sites. We also detected broad adipocyte-specific enrichment of H3K4me2/me1 across this upstream region.

To test whether the distal open chromatin marks identified adipocyte-specific enhancers, we performed transient reporter assays in L1 preadipocytes and adipocytes. We cloned 21 ~1 kb sequences that overlapped the six adipocyte-specific H3K27ac regions, as well as most distal H3K4me2/me1 regions, and 17 additional sequences without any ChIP enrichment as negative controls (Table S5). Each cloned sequence was inserted into three different plasmids carrying a luciferase gene downstream of P2, P3, or no promoter (114 distinct plasmids). Plasmids with no promoter showed uniformly low reporter expression, suggesting that the distal regions possess little intrinsic promoter activity (Figure S5B). Plasmids with P2 or P3 showed reporter expression levels that were positively correlated with the ChIP enrichment scores of the distal regions from which they contained sequences (Figure S6). In particular, sequences from six distinct regions (E1–E6) enhanced the activity of P3 ≥ 2-fold in adipocytes (Figure 4B). Of note, these

(E) Fractions of genes that showed ≥ 2-fold upregulation (left) or downregulation (right) in hASCs, conditional on the maximal enrichment score of associated H3K27ac regions.
(F) Fractions of genes that showed ≥ 2-fold upregulation (left) or downregulation (right) in hASCs, conditional on the number of associated H3K27ac regions.
(G) Fraction of genes associated with at least one adipocyte-specific H3K27ac region in L1s or hASCs, conditional on the ratio of their changes in expression levels during L1 and hASC adipogenesis.
See also Figure S3 and Table S3.

A

PPARγ

	ChIP Enrichment Quartile	Median	Promoter proximal (%)	Motif match (%)	H3K4me/ H3K27ac (Ad, %)	H3K4me/ H3K27ac (Pre, %)	Orthologous region found (%)	Detected in orthologous region (%)
L1 (day 7) n = 7,142	4th	44.0	20.1	82.1	98.0	82.2	84.5	29.9
	3rd	23.3	22.1	68.7	96.0	75.9	82.6	18.4
	2nd	17.9	26.5	56.2	92.6	73.9	80.2	19.4
	1st	13.2	30.2	48.9	91.3	75.2	80.0	17.4
hASC (day 9) n = 39,986	4th	55.0	8.6	67.3	91.8	79.0	77.8	6.9
	3rd	28.1	10.8	48.6	84.9	74.7	76.6	3.2
	2nd	19.3	12.3	39.8	81.4	72.8	75.6	2.7
	1st	13.8	16.3	31.9	84.1	77.3	75.8	2.8

B

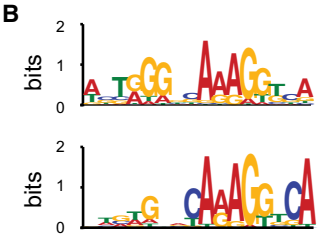

C

Human regions orthologous to L1 PPARγ binding sites

		Bound in hASCs: Yes	Bound in hASCs: No
Motif match	Yes	833	1,426
	No	687	2,900
H3K4me/ H3K27ac	Yes	1,430	2,172
	No	90	2,154

D

	PPARγ		Y	Y	Y	Y	N
	Orthologous		Y	Y	N	N	N
	Dynamic		Y	N	Y	N	N
L1	All	Total (n)	367	767	896	1,925	11,248
		Up (%)	29.7	16.3	18.4	12.2	5.2
	4th quartile	Total (n)	135	316	369	508	13,875
		Up (%)	36.3	24.7	26.8	19.3	6.5
hASC	All	Total (n)	282	848	915	7,580	5,958
		Up (%)	31.6	9.6	17.4	5.0	1.4
	4th quartile	Total (n)	111	426	472	3,687	10,932
		Up (%)	35.1	20.0	22.0	8.3	2.4

E

	Dynamic PPARγ site in: Both	hASC only	L1 only
Total (n)	195	714	807
Up in L1 (%)	28.2	11.1	20.5
Up in hASC (%)	36.4	18.9	7.2

F

Enriched Annotation Categories	p-value
PPARγ sites and up-regulated in L1 + hASC	
PPAR signaling pathway (KEGG)	2×10^{-9}
Lipid metabolism	1×10^{-5}
Lipid homeostasis	3×10^{-4}
Peroxisome	4×10^{-4}
Mitochondrion	6×10^{-4}
Regulation of inflammatory response	4×10^{-3}
PPARγ site and up in L1 only	
Oxioreductase	8×10^{-3}
PPARγ site and up in hASC only	
Glycoprotein	4×10^{-7}
Lipid synthesis	5×10^{-3}

G

CTCF

	ChIP Enrichment Quartile	Median	Promoter proximal (%)	Motif match (%)	H3K4me/ H3K27ac (Ad, %)	Bound in Pre (%)	Orthologous region found (%)	Detected in orthologous region (%)
L1 (day 7) n = 42,957	4th	311.1	10.9	94.9	43.1	99.9	83.3	66.5
	3rd	104.7	11.3	88.7	29.8	98.4	76.3	47.0
	2nd	41.9	11.7	79.4	25.3	86.0	61.2	20.7
	1st	20.0	12.5	70.1	27.8	51.4	52.1	10.9
hASC (day 9) n = 44,717	4th	328.5	11.1	87.6	61.2	99.9	81.2	63.3
	3rd	135.2	11.1	77.9	48.7	99.8	78.0	45.3
	2nd	51.7	13.8	61.2	43.1	94.2	72.5	22.5
	1st	20.5	17.6	39.8	47.1	68.4	69.7	10.3

H

I

Human regions orthologous to L1 CTCF binding sites

		Bound in hASCs: Yes	Bound in hASCs: No
Motif match	Yes	12,840	1,961
	No	2,787	11,769
H3K4me/ H3K27ac	Yes	8,702	4,057
	No	6,925	9,673

Figure 3. PPARγ and CTCF Localization in Adipocytes

(A) Summary of PPARγ-binding sites in L1 and hASC adipocytes. For each quartile of ChIP enrichment scores, the columns show (from left to right) the percentage of sites located ≤ 2 kb from a known promoter; sites overlapping a PPARγ motif; sites overlapping H3K4me3/me2/me1 and/or H3K7ac in adipocytes and in preadipocytes; sites that could be mapped to an orthologous region in the other genome; and mapped sites that were also bound by PPARγ in the other model.

(B) Motifs learned ab initio from sequences ± 100 bp from the top 800 PPARγ-binding sites in L1s (ranked by enrichment scores). Virtually identical motifs were learned from hASCs.

(C) Correlations between PPARγ binding, the presence of a conserved motif instance, and open chromatin marks in human genomic regions orthologous to L1 PPARγ-binding sites.

(D) Fractions of genes that were upregulated ≥ 2-fold in L1s or hASCs, conditional on association with a PPARγ-binding site. Orthologous PPARγ-binding sites could be mapped to an orthologous region also bound in the other model. Dynamic PPARγ-binding sites increased H3K27ac enrichment ≥ 5-fold.

(E) Fractions of genes that were upregulated ≥ 2-fold in L1s or hASCs, conditional on association with dynamic PPARγ-binding sites.

(F) Annotation enrichment analysis of orthologs associated with PPARγ-binding sites and upregulated ≥ 2-fold. p values are Benjamini corrected.

(G) Summary of CTCF-binding sites in L1 and hASC adipocytes.

(H) Motif learned ab initio from sequences ± 100 bp from the top 800 CTCF-binding sites in L1s (ranked by enrichment scores). A virtually identical motif was learned from hASCs.

(I) Correlations between CTCF binding, the presence of a conserved motif instance, and open chromatin marks in human genomic regions orthologous to L1 CTCF-binding sites.

See also Figure S4 and Table S4.

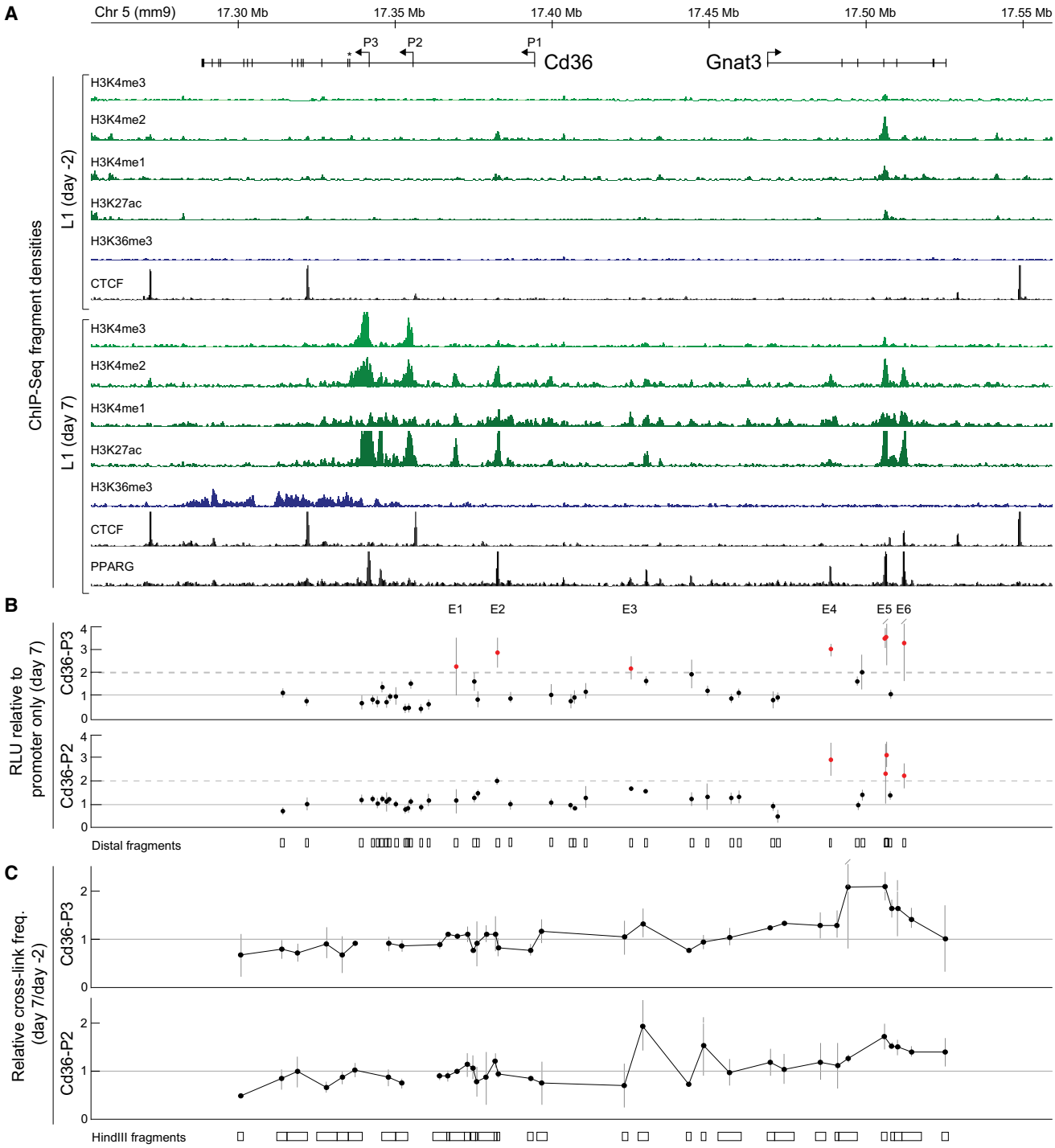

Figure 4. Identification of Adipocyte-Specific Cd36 *cis*-Regulatory Elements

(A) Chromatin state maps of the ~300 kb *Cd36/Gnat3* locus from L1 preadipocytes (day −2) and adipocytes (day 7). *Cd36* has three known promoters (P1–P3). (Asterisk) Start of the protein-coding sequence.

(B) Reporter assays. Each dot shows the ratio of normalized luciferase expression (RLU) from plasmids carrying distal fragments upstream of P2 or P3 over the estimated basal activity of the promoter. Fragments from six distinct distal sites (E1–E6) showed ≥ 2-fold mean enhancement of expression from P3 (orange dots, top). Three of these (orange dots, bottom) also showed ≥ 2-fold mean enhancement of expression from P2. E5 was present within two overlapping fragments. Error bars show standard errors of the means.

(C) Chromosome conformation capture. Each dot shows the cross-linking frequency of a HindIII fragment to P3 (top) or P2 (bottom) in adipocytes relative to preadipocytes. Error bars show standard errors of the means.

See also Figure S5, Figure S6, and Table S5.

corresponded to five of the six distal adipocyte-specific H3K27ac regions, whereas the sixth (E3) was primarily enriched for H3K4me1. Sequences from E4–E6 also enhanced the activity of P2 $\geq$ 2-fold in adipocytes. By contrast, only one plasmid (E5 upstream of P2) showed comparable enhancer activity in preadipocytes. This confirms that dynamic H3K27ac enrichment is a signature of cell type-specific enhancers.

To determine whether E1–E6 physically interact with P2 and P3 in their native chromatin context (Ptashne, 1986), we used chromosome conformation capture (Dekker et al., 2002). We found that the frequency of interactions between the two promoters and E3–E6, which are located 75–150 kb upstream, increased ~2-fold in adipocytes relative to preadipocytes (Figure 4C and Table S5). E1 and E2, which are located much closer to the promoters, also showed consistent but less-significant (~1.1-fold) changes. We conclude that *Cd36* is regulated by multiple distal enhancers, including three that are located within introns of the neighboring gene *Gnat3*.

We next compared the murine *Cd36* locus to human *CD36* (Figure 5A). All three murine promoters were conserved in the human genome. In contrast to L1s, however, we only detected H3K4me3 at P3, indicating that this is the major promoter used in hASCs.

Three of the six enhancers identified in L1s (E2, E4, and E6) were shared with hASCs. Of the three L1-specific enhancers, E1 and E3 were located in nonrepetitive sequences in the mouse genome but had no recognizable orthologs in human. Most of the E5 sequence could be mapped, but the chromatin marks across this ~1 kb region in L1s were not shared with hASCs. Upon close inspection, we found that the PPARγ motif in E5 in the mouse genome was located in a small (~100 bp) fragment of a rodent-specific LINE/L1 transposon (Figure 5B). Insertion of this element therefore appears to have generated a species-specific PPRE. Conversely, we detected at least two putative enhancers/PPREs in hASCs (based on H3K27ac and PPARγ enrichment) that could not be mapped to the murine genome.

Two of the three distal CTCF-binding sites in L1s were also shared with hASCs. The third site, located upstream of E6, could be mapped to an orthologous region that was not bound in hASCs (Figure 5C). CTCF did, however, bind to a site ~5 kb away in hASCs that was not shared with L1s. Inspection revealed that the CTCF motif bound in L1s was not conserved in the human genome and vice versa (Figure 5D). Thus, the approximate location of this putative insulator element appears to be conserved even though the specific motif instances are not. We conclude that, whereas the overall regulatory architecture of the *Cd36*/*CD36* locus is conserved, there has been substantial turnover of specific *cis*-regulatory elements.

Identification of Previously Unidentified *trans*-Regulatory Factors

Finally, we explored whether we could use the chromatin state maps to identify *trans*-regulatory factors in the adipogenic GRN. L1s and hASCs each express hundreds of sequence-specific TFs, not all of which are likely to be directly involved in adipogenesis. Whereas our data show that many active *cis*-regulatory elements are not shared, the identities and sequence specificities of the factors that interact with them are likely to be better conserved (Weirauch and Hughes, 2010). Accordingly, we enumerated instances of all known TF motifs within regions that underwent chromatin remodeling in L1s or hASCs and then ranked the motifs according to their relative enrichment in adipocyte- or preadipocyte-specific regions. Strikingly, many of the most enriched motifs from both models corresponded to known pro- and anti-adipogenic regulatory factors (Table S6).

Figure 6 shows the most enriched motifs in regions that (1) gained or lost H3K27ac during L1 adipogenesis and (2) could be mapped to orthologous regions with the same mark in hASCs. Each of these motifs was enriched in both the mouse and the orthologous human sequence. Among the motifs most enriched within adipocyte-specific H3K27ac regions are those recognized by PPARγ/RXR and C/EBP proteins, which together form the core adipogenic GRN. The list of motifs also contained other known regulators of adipogenesis, such as the IRF, GATA, NF-κB, and STAT families. The motifs most enriched within preadipocyte-specific H3K27ac regions are recognized by several mediators of growth factor responses and regulators of cell proliferation, such as AP-1 (FOS/JUN), SRF, and MEF2A, as well as a variety of developmental factors from the homeodomain and POU families.

The presence of multiple known regulators near the top of the ranked motif lists suggested that other TFs with similar ranks but no previous evidence of involvement in adipogenesis are good candidates for follow-up. We selected two of these factors for further analysis: promyelocytic leukemia zinc finger protein (PLZF, encoded by *Zbtb16*) and serum response factor (SRF, encoded by *Srf*). Expression of both of these factors was detected in our L1 and hASC microarray data. We also confirmed their expression in mouse adipose tissue and differentiating L1 cells using RT-qPCR (Figure S7). To assess whether these factors regulate adipogenesis, we used gain- and loss-of-function assays. We found that independent overexpression of either factor in L1 cells (Figure S7) was sufficient to repress adipogenesis, as evidenced by reduced lipid accumulation (Figure 7A) and diminished markers of terminal differentiation (Figures 7B and 7C). Conversely, RNAi-mediated knockdown of PLZF or SRF (Figure S7) enhanced L1 adipogenesis, as assessed by the same parameters (Figures 7D–7F). Similar effects were obtained with two unique hairpins for each factor. These data indicate that *trans*-regulatory factors in GRNs can be identified by an integrated approach incorporating epigenomic profiling and motif enrichment analysis.

DISCUSSION

We have generated comparative chromatin state maps, TF localization maps, and gene expression profiles from differentiating L1s and hASCs. Our initial analysis of the data demonstrates their utility to studies of chromatin remodeling and gene regulation in adipogenesis and cellular differentiation.

Comparisons between time points revealed a close correlation between changes in gene expression and changes in distal open chromatin marks. Whereas only a minority of regions enriched for H3K27ac changed during adipogenesis, this dynamic subset appeared to be highly enriched for adipocyte

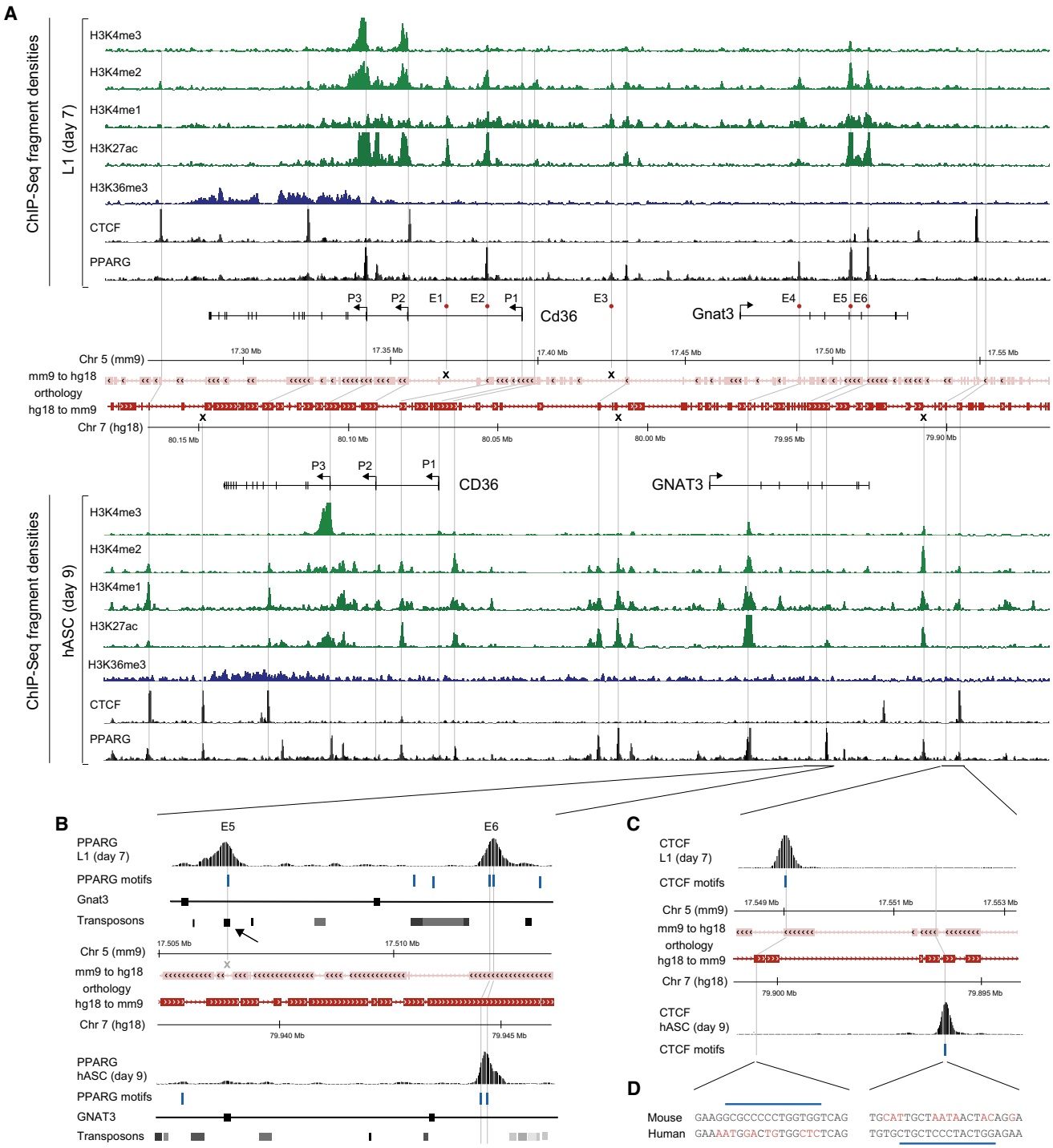

Figure 5. Comparison of Cd36/CD36 in L1 and hASC Adipocytes

(A) Genomic and chromatin state maps from L1 (top) and hASC (bottom) adipocytes. Orthology tracks show regions mapped from the mouse to the human genome (pink) and vice versa (red). Gray vertical lines highlight orthologous sites, those terminated by X highlight sites that could not be mapped. Orange dots show the E1–E6 enhancers identified in L1s.

(B) Expanded view of E5/E6 shows the locations of PPARγ motifs (blue bars) and transposons (gray/black) in the genomic sequences. The PPARγ motif underlying the peak of the L1 ChIP-Seq signal lies within a rodent-specific LINE/L1 fragment (arrow).

(C) Expanded view of an upstream region shows CTCF ChIP-Seq signals at nonorthologous sites separated by ~2.4–5 kb in L1s and hASCs.

(D) Alignments of the sequences underlying the two nonorthologous sites in (C) show that the underlying motifs (blue bars) are not conserved.

Enriched in pre-adipocyte -specific H3K27ac

Motif	ID	Ratio	Candidates
	U_Pou3f3	0.32	?
	U_Cphx	0.34	?
	U_Hoxa6	0.36	Homeobox-family
	M00026	0.41	Mef2a
	U_Tbp	0.44	Tbp
	U_Srf	0.46	Srf
	M00495	0.52	Bach1/2
	M00199	0.54	Fos/Jun (AP-1)
	M00987	0.55	Foxp1
	M00795	0.56	Pou2f1 (Octamer motif)
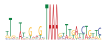	M01075	0.57	Zbtb16 (PLZF)
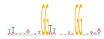	M00999	0.60	?
	U_Tcf7	0.62	Tcf7l2, Tcf3, Lef1
	M00747	0.62	Irf1/3
	M01146	0.62	?
	M00920	0.63	E2f
	M00498	0.63	(Stat half-site)
	U_Evx2	0.65	Homeobox-family
	M00694	0.67	E4f1
	U_Hoxa13	0.71	Homeobox-family

Enriched in adipocyte-specific H3K27ac

Motif	ID	Ratio	Candidates
	M00278	2.1	Gata-family
	M01132	2.1	Rxra/b + others (NHR half-site)
	M00240	1.9	? (Nkx2 family)
	M00117	1.8	Cebpa/b/d/g/z
	M00526	1.8	Nr6a1
	M00539	1.6	Max, Myc + others (E box)
	U_Zfp161	1.6	Zfp161
	M00191	1.6	Rxra/b + others (NHR half-site)
	M01069	1.6	Gzf1
	U_Irf4	1.6	Irf3/4/5/6
	M00237	1.6	Ahr:Arnt dimer
	U_Gmeb1	1.6	Gmeb1
	M00105	1.5	Cux1
	M00651	1.5	Nfkb1
	M00979	1.5	?
	M00963	1.5	Rxra/b + others (NHR half-site)
	M00196	1.4	Sp1 + others (G/C-box)
	M00040	1.4	Atf2
	U_Rxra	1.4	Rxra/b + others (NHR half-site)
	U_Osr2	1.3	Osr1/2

Figure 6. TF Motifs Associated with Chromatin Remodeling during Adipogenesis

TF motifs with the highest relative enrichment in adipocyte- (right) and preadipocyte-specific (left) H3K27ac regions. The top 400 L1 adipocyte and preadipocyte H3K27ac regions (ranked by enrichment scores) that could be mapped to orthologous locations with H3K27ac in hASCs were used. Each mammalian TRANSFAC (M prefix) and UniPROBE (U prefix) motif was matched and assigned adipocyte/preadipocyte enrichment ratios in the underlying mouse and human sequences (corrected for length and composition). The "ratio" columns show the maximal (left) or minimal (right) enrichment ratio from mouse and human for nonredundant motifs with consistent enrichment ratios in the two genomes. The "candidates" columns show genes or gene families expressed in L1 cells that are known to recognize each of the motifs. See also Table S6.

and preadipocyte-specific enhancers. Thus, profiling chromatin states before and after induction of a phenotype of interest can help pinpoint regulatory elements that are directly related to that phenotype. Importantly, gain of histone acetylation might help to distinguish functional PPREs from nonproductive PPARγ-binding sites. Similar observations were recently reported for endotoxin- and androgen-responsive enhancers in macrophages (Ghisletti et al., 2010) and prostate cancer cells (He et al., 2010), respectively. We also found that dynamically expressed genes were often associated with multiple distal elements that showed coordinated changes in chromatin state. Elucidating how these distinct elements interact with each other and their target genes will be important to our understanding of mammalian gene regulation.

Comparisons between the two models revealed significant overlaps of chromatin marks in orthologous regions, which is consistent with a previous study of mouse and human fibroblasts (Bernstein et al., 2005). The majority of open chromatin marks and TF-binding sites were, however, not shared. Strikingly, differential recruitment of PPARγ and CTCF was correlated with turnover of their motifs. This suggests that many model-specific TF-binding sites and associated chromatin marks reflect genetic divergence between mouse and human, rather than ontogenetic or technical differences between L1s and hASCs. Similar turnover has recently been observed in hepatocytes (Odom et al., 2007; Schmidt et al., 2010). Of interest, many TF-binding sites that could not be mapped between the genomes were located within lineage-specific transposon insertions, which is consistent with transposons being a major creative force in the evolution of mammalian gene regulation (Lowe et al., 2007; Mikkelsen et al., 2007b). A key remaining question is to what extent turnover of TF-binding sites reflects adaptation, or simply GRN "drift," that may affect expression levels but has no significant biological impact. Importantly, we found that orthologs targeted by PPARγ in both models were enriched for functions relevant to known adipocyte biology. Moreover, analysis of the orthologous *Cd36/CD36* loci revealed multiple species-specific regulatory elements, despite their similar expression patterns. The presence of multiple distal regulatory elements with similar activities near a single gene might facilitate turnover of individual elements by providing redundancy.

Finally, motif enrichment analysis revealed that the close relationship between chromatin state and TF-binding sites can be utilized to infer previously unidentified *trans*-regulators. We previously identified roles for interferon regulatory factors (IRFs) and the orphan nuclear receptor COUP-TFII in adipogenesis based on analysis of chromatin at a limited number of loci (Eguchi et al., 2008; Xu et al., 2008). Using our genome-wide data, we discovered two additional factors, PLZF and SRF, with anti-adipogenic activity. PLZF is a member of the BTB/POZ domain family of TFs (Kelly and Daniel, 2006) and appears to function primarily as a repressor by recruiting nuclear receptor corepressors (N-CoRs) and histone deacetylases (HDACs). SRF is a MADS box TF originally named for its role in mediating the effects of serum stimulation (Norman et al., 1988). We are currently attempting to understand the specific functions of PLZF and SRF in adipogenesis. In addition, we are using the

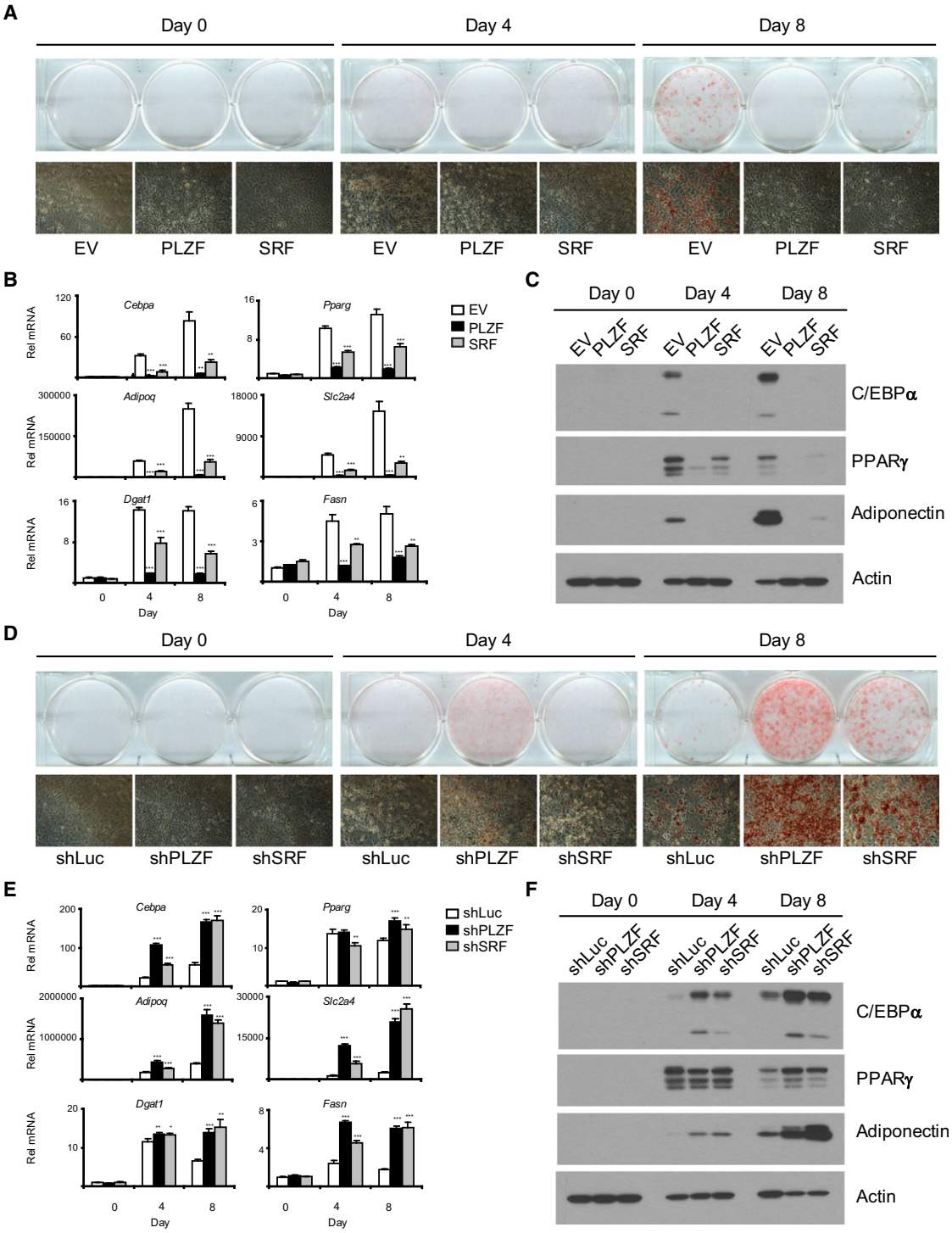

Figure 7. PLZF and SRF Regulate Adipogenesis

(A) L1 preadipocytes were transduced with retrovirus expressing PLZF or SRF (pMSCV empty vector [EV] as control) and induced to differentiate. The cells were subjected to oil red O staining at the indicated time points.

(B) mRNA levels relative to 36B4 were assessed by RT-qPCR (mean ± SD; n = 4) at the indicated time points. **p < 0.01; ***p < 0.001.

(C) Protein levels were assessed by western blotting at the indicated time points.

(D) L1 preadipocytes were transduced with a retrovirus expressing control shRNA (shLuc), PLZF (shPLZF), or SRF (shSRF). The cells were subjected to oil red O staining at the indicated time points.

(E) mRNA levels relative to 36B4 were assessed by RT-qPCR (mean ± SD; n = 4) at the indicated time points. *p < 0.05; **p < 0.01; ***p < 0.001.

(F) Protein levels were assessed by western blotting at the indicated time points. See also Figure S7.

chromatin state maps to identify other factors in the adipogenic GRN. This approach can be expected to become increasingly powerful as the completeness and quality of TF motif databases improve. More generally, we expect that it can be applied to studies of a variety of other gene regulatory networks.

EXPERIMENTAL PROCEDURES

Oligonucleotides and Antibodies

All primers, hybridization probes, hairpin sequences, and antibodies used are listed in Table S7 and the Extended Experimental Procedures.

Cell Culture

3T3-L1 cells were cultured and differentiated as described in Eguchi et al. (2008). Human abdominal adipose tissue was obtained with informed consent from a 33-year-old Caucasian female (BMI = 32.96 Kg/m^2) undergoing lipoaspiration (Pennington Biomedical Research Center Institutional Review Board, Protocol PBRC24030). hASCs were isolated as described in Dubois et al. (2008) and differentiated using a protocol modified from Hebert et al. (2009). For additional details, see the Extended Experimental Procedures.

ChIP-Seq

L1 cells and hASCs were treated with 1% formaldehyde for 10 min at 37°C and stored at −80°C. ChIP and Illumina sequencing library construction were performed as described in Mikkelsen et al. (2007a). The computational analysis is described in the Extended Experimental Procedures.

RNA Preparation and Expression Analysis

Total RNA was prepared using TRIzol (Invitrogen). mRNA expression data were generated using GeneChip arrays (Affymetrix). miRNA expression data were generated using BeadChips (Illumina). RT-qPCR were performed using SuperScript III (Invitrogen) or RETROscript kit (Ambion), SYBR Green, and the 7900HT Real-Time PCR system (Applied Biosystems). Annotation enrichment analysis was performed using DAVID 6.7 (Dennis et al., 2003).

Reporter Assays

Cd36 P2, P3, and 38 distal sequences were PCR amplified from a BAC (RP23-175A11; BACPAC Resource Center) and cloned into pGL4.10 (Promega) using In-Fusion (Clontech). L1 cells were nucleofected with solution SE (Lonza) and the FF-150 and DS-137 programs for preadipocytes and adipocytes, respectively. Luciferase activities were measured using Dual-Glow (Promega) and an EnVision 2103 multilabel reader (PerkinElmer).

Chromosome Conformation Capture

Chromosome conformation capture (3C) was performed using RT-qPCR with FAM/IBFQ hybridization probes (IDT) and HindIII digestion as described in Hagège et al. (2007). The normalization library was generated from the RP23-175A11 BAC.

Sequence Analysis

All sequence analyses were performed on the hg18 (human) and mm9 (mouse) reference genome sequences and annotations (http://genome.ucsc.edu). Orthologous regions were mapped using liftOver (UCSC), requiring > 10% nucleotide overlap. Motif discovery was performed using MEME 4.3 (Bailey and Elkan, 1994). Motif instance matching was performed using FIMO with a p value threshold of 10^{-4}. The motif enrichment analysis was performed using TRANSFAC 11.3 and UniPROBE (Oct 7, 2009), as described in the Extended Experimental Procedures.

PLZF and SRF Overexpression and Knockdown

ORFs were PCR amplified and cloned into pMSCV (Clontech). shRNAs were synthesized and cloned into pSIREN (Clontech). Retroviruses were generated using Phoenix cells and CellPhect (Amersham Biosciences) and were used to transduce L1 preadipocyte subclones that typically differentiate at 30%–50% efficiency. For additional details, see the Extended Experimental Procedures.

ACCESSION NUMBERS

All microarray expression and sequencing data have been deposited to the NCBI GEO database (http://www.ncbi.nlm.nih.gov/geo/) under accession number GSE20752.

SUPPLEMENTAL INFORMATION

Supplemental Information includes Extended Experimental Procedures, seven figures, and seven tables and can be found with this article online at doi:10.1016/j.cell.2010.09.006.

ACKNOWLEDGMENTS

The authors would like to thank the staff of the Broad Institute for assistance with data generation and Gang Yu at the Tissue Culture Core Facility, Pennington Biomedical Research Center, for isolating the hASCs. This project was supported by funds from the Broad Institute, NIH DK63906 (E.D.R.), an American Diabetes Association Career Development Award (E.D.R.), the Pennington Biomedical Research Foundation (J.M.G.), and NORC Center Grant #1P30 DK072476 (J.M.G.). J.M.G. declares that he has consulted for companies focusing on adipose-derived adult stem cells (Toucan Capital, Cognate Bioservices, Vet-Stem) and has cofounded companies involved in developing these cells for clinical applications.

Received: April 17, 2010
Revised: July 13, 2010
Accepted: August 27, 2010
Published: September 30, 2010

REFERENCES

Arnone, M.I., and Davidson, E.H. (1997). The hardwiring of development: organization and function of genomic regulatory systems. Development *124*, 1851–1864.

Aust, L., Devlin, B., Foster, S.J., Halvorsen, Y.D., Hicok, K., du Laney, T., Sen, A., Willingmyre, G.D., and Gimble, J.M. (2004). Yield of human adipose-derived adult stem cells from liposuction aspirates. Cytotherapy *6*, 7–14.

Bailey, T.L., and Elkan, C. (1994). Fitting a mixture model by expectation maximization to discover motifs in biopolymers. Proc. Int. Conf. Intell. Syst. Mol. Biol. *2*, 28–36.

Barski, A., Cuddapah, S., Cui, K., Roh, T.Y., Schones, D.E., Wang, Z., Wei, G., Chepelev, I., and Zhao, K. (2007). High-resolution profiling of histone methylations in the human genome. Cell *129*, 823–837.

Bernstein, B.E., Kamal, M., Lindblad-Toh, K., Bekiranov, S., Bailey, D.K., Huebert, D.J., McMahon, S., Karlsson, E.K., Kulbokas, E.J., III, Gingeras, T.R., et al. (2005). Genomic maps and comparative analysis of histone modifications in human and mouse. Cell *120*, 169–181.

Birney, E., Stamatoyannopoulos, J.A., Dutta, A., Guigó, R., Gingeras, T.R., Margulies, E.H., Weng, Z., Snyder, M., Dermitzakis, E.T., Thurman, R.E., et al; ; ENCODE Project Consortium. (2007). Identification and analysis of functional elements in 1% of the human genome by the ENCODE pilot project. Nature *447*, 799–816.

Camp, H.S., Ren, D., and Leff, T. (2002). Adipogenesis and fat-cell function in obesity and diabetes. Trends Mol. Med. *8*, 442–447.

Dekker, J., Rippe, K., Dekker, M., and Kleckner, N. (2002). Capturing chromosome conformation. Science *295*, 1306–1311.

Dennis, G., Jr., Sherman, B.T., Hosack, D.A., Yang, J., Gao, W., Lane, H.C., and Lempicki, R.A. (2003). DAVID: Database for Annotation, Visualization, and Integrated Discovery. Genome Biol. *4*, P3.

Dubois, S.G., Floyd, E.Z., Zvonic, S., Kilroy, G., Wu, X., Carling, S., Halvorsen, Y.D., Ravussin, E., and Gimble, J.M. (2008). Isolation of human adipose-derived stem cells from biopsies and liposuction specimens. Methods Mol. Biol. *449*, 69–79.

Eguchi, J., Yan, Q.W., Schones, D.E., Kamal, M., Hsu, C.H., Zhang, M.Q., Crawford, G.E., and Rosen, E.D. (2008). Interferon regulatory factors are transcriptional regulators of adipogenesis. Cell Metab. *7*, 86–94.

Ghisletti, S., Barozzi, I., Mietton, F., Polletti, S., De Santa, F., Venturini, E., Gregory, L., Lonie, L., Chew, A., Wei, C.L., et al. (2010). Identification and characterization of enhancers controlling the inflammatory gene expression program in macrophages. Immunity *32*, 317–328.

Green, H., and Meuth, M. (1974). An established pre-adipose cell line and its differentiation in culture. Cell *3*, 127–133.

Hagège, H., Klous, P., Braem, C., Splinter, E., Dekker, J., Cathala, G., de Laat, W., and Forné, T. (2007). Quantitative analysis of chromosome conformation capture assays (3C-qPCR). Nat. Protoc. *2*, 1722–1733.

He, H.H., Meyer, C.A., Shin, H., Bailey, S.T., Wei, G., Wang, Q., Zhang, Y., Xu, K., Ni, M., Lupien, M., et al. (2010). Nucleosome dynamics define transcriptional enhancers. Nat. Genet. *42*, 343–347.

Hebert, T.L., Wu, X., Yu, G., Goh, B.C., Halvorsen, Y.D., Wang, Z., Moro, C., and Gimble, J.M. (2009). Culture effects of epidermal growth factor (EGF) and basic fibroblast growth factor (bFGF) on cryopreserved human adipose-derived stromal/stem cell proliferation and adipogenesis. J. Tissue Eng. Regen. Med. *3*, 553–561.

Heintzman, N.D., Hon, G.C., Hawkins, R.D., Kheradpour, P., Stark, A., Harp, L.F., Ye, Z., Lee, L.K., Stuart, R.K., Ching, C.W., et al. (2009). Histone modifications at human enhancers reflect global cell-type-specific gene expression. Nature *459*, 108–112.

Hon, G.C., Hawkins, R.D., and Ren, B. (2009). Predictive chromatin signatures in the mammalian genome. Hum. Mol. Genet. *18*(R2), R195–R201.

IJpenberg, A., Jeannin, E., Wahli, W., and Desvergne, B. (1997). Polarity and specific sequence requirements of peroxisome proliferator-activated receptor (PPAR)/retinoid X receptor heterodimer binding to DNA. A functional analysis of the malic enzyme gene PPAR response element. J. Biol. Chem. *272*, 20108–20117.

Johnson, D.S., Mortazavi, A., Myers, R.M., and Wold, B. (2007). Genome-wide mapping of in vivo protein-DNA interactions. Science *316*, 1497–1502.

Kelly, K.F., and Daniel, J.M. (2006). POZ for effect—POZ-ZF transcription factors in cancer and development. Trends Cell Biol. *16*, 578–587.

Kim, T.H., Abdullaev, Z.K., Smith, A.D., Ching, K.A., Loukinov, D.I., Green, R.D., Zhang, M.Q., Lobanenkov, V.V., and Ren, B. (2007). Analysis of the vertebrate insulator protein CTCF-binding sites in the human genome. Cell *128*, 1231–1245.

Lefterova, M.I., Zhang, Y., Steger, D.J., Schupp, M., Schug, J., Cristancho, A., Feng, D., Zhuo, D., Stoeckert, C.J., Jr., Liu, X.S., and Lazar, M.A. (2008). PPARgamma and C/EBP factors orchestrate adipocyte biology via adjacent binding on a genome-wide scale. Genes Dev. *22*, 2941–2952.

Lowe, C.B., Bejerano, G., and Haussler, D. (2007). Thousands of human mobile element fragments undergo strong purifying selection near developmental genes. Proc. Natl. Acad. Sci. USA *104*, 8005–8010.

Mikkelsen, T.S., Ku, M., Jaffe, D.B., Issac, B., Lieberman, E., Giannoukos, G., Alvarez, P., Brockman, W., Kim, T.K., Koche, R.P., et al. (2007a). Genome-wide maps of chromatin state in pluripotent and lineage-committed cells. Nature *448*, 553–560.

Mikkelsen, T.S., Wakefield, M.J., Aken, B., Amemiya, C.T., Chang, J.L., Duke, S., Garber, M., Gentles, A.J., Goodstadt, L., Heger, A., et al.Broad Institute Genome Sequencing Platform; Broad Institute Whole Genome Assembly Team. (2007b). Genome of the marsupial Monodelphis domestica reveals innovation in non-coding sequences. Nature *447*, 167–177.

Nielsen, R., Pedersen, T.A., Hagenbeek, D., Moulos, P., Siersbaek, R., Megens, E., Denissov, S., Børgesen, M., Francoijs, K.J., Mandrup, S., and Stunnenberg, H.G. (2008). Genome-wide profiling of PPARgamma:RXR and RNA polymerase II occupancy reveals temporal activation of distinct metabolic pathways and changes in RXR dimer composition during adipogenesis. Genes Dev. *22*, 2953–2967.

Noer, A., Lindeman, L.C., and Collas, P. (2009). Histone H3 modifications associated with differentiation and long-term culture of mesenchymal adipose stem cells. Stem Cells Dev. *18*, 725–736.

Norman, C., Runswick, M., Pollock, R., and Treisman, R. (1988). Isolation and properties of cDNA clones encoding SRF, a transcription factor that binds to the c-fos serum response element. Cell *55*, 989–1003.

Odom, D.T., Dowell, R.D., Jacobsen, E.S., Gordon, W., Danford, T.W., MacIsaac, K.D., Rolfe, P.A., Conboy, C.M., Gifford, D.K., and Fraenkel, E. (2007). Tissue-specific transcriptional regulation has diverged significantly between human and mouse. Nat. Genet. *39*, 730–732.

Phillips, J.E., and Corces, V.G. (2009). CTCF: master weaver of the genome. Cell *137*, 1194–1211.

Ptashne, M. (1986). Gene regulation by proteins acting nearby and at a distance. Nature *322*, 697–701.

Robertson, G., Hirst, M., Bainbridge, M., Bilenky, M., Zhao, Y., Zeng, T., Euskirchen, G., Bernier, B., Varhol, R., Delaney, A., et al. (2007). Genome-wide profiles of STAT1 DNA association using chromatin immunoprecipitation and massively parallel sequencing. Nat. Methods *4*, 651–657.

Rosen, E.D., and MacDougald, O.A. (2006). Adipocyte differentiation from the inside out. Nat. Rev. Mol. Cell Biol. *7*, 885–896.

Rosen, E.D., and Spiegelman, B.M. (2006). Adipocytes as regulators of energy balance and glucose homeostasis. Nature *444*, 847–853.

Schmidt, D., Wilson, M.D., Ballester, B., Schwalie, P.C., Brown, G.D., Marshall, A., Kutter, C., Watt, S., Martinez-Jimenez, C.P., Mackay, S., et al. (2010). Five-vertebrate ChIP-seq reveals the evolutionary dynamics of transcription factor binding. Science *328*, 1036–1040.

Valouev, A., Johnson, D.S., Sundquist, A., Medina, C., Anton, E., Batzoglou, S., Myers, R.M., and Sidow, A. (2008). Genome-wide analysis of transcription factor binding sites based on ChIP-Seq data. Nat. Methods *5*, 829–834.

Wang, Z., Zang, C., Rosenfeld, J.A., Schones, D.E., Barski, A., Cuddapah, S., Cui, K., Roh, T.Y., Peng, W., Zhang, M.Q., and Zhao, K. (2008). Combinatorial patterns of histone acetylations and methylations in the human genome. Nat. Genet. *40*, 897–903.

Weirauch, M.T., and Hughes, T.R. (2010). Conserved expression without conserved regulatory sequence: the more things change, the more they stay the same. Trends Genet. *26*, 66–74.

Xi, H., Shulha, H.P., Lin, J.M., Vales, T.R., Fu, Y., Bodine, D.M., McKay, R.D., Chenoweth, J.G., Tesar, P.J., Furey, T.S., et al. (2007). Identification and characterization of cell type-specific and ubiquitous chromatin regulatory structures in the human genome. PLoS Genet. *3*, e136.

Xu, Z., Yu, S., Hsu, C.H., Eguchi, J., and Rosen, E.D. (2008). The orphan nuclear receptor chicken ovalbumin upstream promoter-transcription factor II is a critical regulator of adipogenesis. Proc. Natl. Acad. Sci. USA *105*, 2421–2426.

Yu, S., Matsusue, K., Kashireddy, P., Cao, W.Q., Yeldandi, V., Yeldandi, A.V., Rao, M.S., Gonzalez, F.J., and Reddy, J.K. (2003). Adipocyte-specific gene expression and adipogenic steatosis in the mouse liver due to peroxisome proliferator-activated receptor gamma1 (PPARgamma1) overexpression. J. Biol. Chem. *278*, 498–505.

Zhang, X., Odom, D.T., Koo, S.H., Conkright, M.D., Canettieri, G., Best, J., Chen, H., Jenner, R., Herbolsheimer, E., Jacobsen, E., et al. (2005). Genome-wide analysis of cAMP-response element binding protein occupancy, phosphorylation, and target gene activation in human tissues. Proc. Natl. Acad. Sci. USA *102*, 4459–4464.